Journal of Applied Polymer Science

Enhanced thermal stability of biomedical thermoplastic polyurethane with the addition of cellulose nanocrystals

Jen-Chieh Liu,[1] Darren J. Martin,[2] Robert J. Moon,[1,3,4] Jeffrey P. Youngblood[1]

[1]School of Materials Engineering, Purdue University, West Lafayette, Indiana

[2]Australian Institute of Bioengineering & Technology, University of Queensland, Brisbane 4072, Australia

[3]Forest Products Laboratory, US Forest Service, Madison, Wisconsin

[4]Renewable Bioproducts Institute, Georgia Institute of Technology, Atlanta, Georgia

Correspondence to: R. J. Moon (E-mail: robertmoon@fs.fed.us) and J. P. Youngblood (E-mail: jpyoungb@purdue.edu)

ABSTRACT: Freeze-dried cellulose nanocrystals (CNCs) were dispersed in the thermoplastic polyurethane [Pellethane 2363-55D (P55D)] by a solvent casting method to fabricate CNC-reinforced nanocomposites. This study demonstrated that the addition of small amounts (1–5 wt %) of CNCs to P55D increased the thermal degradation temperature while maintaining a similar stiffness, strength, and elongation of the neat P55D. CNC additions to P55D did not alter the glass-transition temperature, but the onset decomposition temperature was shifted from 286 to 327°C when 1 wt % CNCs was dispersed in the matrix. The higher onset decomposition temperature was attributed to the formation of hydrogen bonds between the hydroxyl groups on the CNC surface and urethane groups in the hard block of P55D. The ultimate tensile strength and strain to failure (ε_f) of the nanocomposites were minimally affected by additions up to 5 wt % CNCs, whereas the elastic modulus was increased by about 70%. The observation that ε_f was unchanged with the addition of up to 5 wt % CNCs suggested that the flow/sliding of the hard blocks and chains were not hindered by the presence of the CNCs during plastic deformation. The ramifications of this study was that CNC additions resulted in wider processing temperatures of P55D for various biomedical devices while maintaining a similar stiffness, strength, and elongation.
 J. Appl. Polym. Sci. **2015**, *132*, 41970.

KEYWORDS: biomedical applications; cellulose and other wood products; composites; polyurethanes; thermoplastics

Received 29 September 2014; accepted 7 January 2015

DOI: 10.1002/app.41970

INTRODUCTION

Thermoplastic polyurethanes (TPUs) are used in the manufacturing of biomedical devices (e.g., endotracheal tubes, vascular grafts, ventricular assistance devices), where the mechanical performance (e.g., controllable stiffness, high strength and ductility) combined with the biocompatibility/nontoxicity of TPUs are important. TPUs are multiblock copolymers consisting of alternating soft and hard segments; they have a phase-separated microstructure because of the thermodynamic incompatibility between the blocks. The flexible soft segment is composed of long-chain diols, and the hard segment is formed by the reaction of diisocyanate, typically with a short diol chain extender. In attempts to broaden the typical property profiles to expand the range of possible applications, various types of functional nanofillers (e.g., carbon nanotubes, layered silicates, nanoclays)[1–3] have been incorporated into TPUs to pursue nanocomposites with better mechanical properties and thermal stability and low gas permeability. However, for biomedical devices, the biocompatibility/nontoxicity of TPU nanocomposites is also very important. Hence, the exploration of nontoxic nanoreinforcements for TPUs is important. Recently, much research has focused on the use of nanoclays or organosilicates as nanofillers in commercial TPUs for biomedical applications; this has successfully improved the mechanical, thermal, and barrier properties and enhanced the dimensional stability of TPUs.[2]

Cellulose nanocrystals (CNCs) may also be a good candidate as nanoreinforcement materials for polymer systems for biocompatible/nontoxicity applications, as they have high mechanical properties [elastic modulus (E) = 110–220 GPa, ultimate tensile strength (σ_T) ≈7.5 GPa],[4] and preliminary studies have shown them to have a low toxicity.[5] CNCs are cellulose-based nanoparticles that are produced from wood or plant fibers via acid hydrolysis.[4] The rodlike particles have high aspect ratios (10–100; width = 3–5 nm, length = 50–500 nm) and a high crystallinity (54–88%).[4] CNCs also have good thermal properties (e.g., thermal degradation temperature ≈ 260°C, low thermal expansion = 2 ppm/K),[4,6] low density (1.6 g/cm^3), low light scattering, and surfaces that can be easily functionalized.[4]

CNC nanocomposites have been produced with a variety of polymer systems, which have demonstrated improved mechanical performance,[4,7,8] optical properties,[9,10] and thermal stability and conductivity.[11–13] Several studies have used CNCs as a reinforcement phase in TPUs.[14–21] In these studies, CNCs were dispersed in the matrix by either a two-step polymerization process[14–16] or were directly blended with already synthesized[17,18] or commercialized[19,20] TPUs. In the two-step polymerization process, CNCs were blended with polyol and isocyanate in the *N,N*-dimethylformamide (DMF) to synthesize TPU prepolymer, and a chain extender was then added to the prepolymer for a continuous reaction. The homogeneous suspension was then allowed to dry to fabricate the CNC nanocomposites. For the direct-blending process, the synthesized TPUs or commercialized TPUs were initially dissolved in DMF, and the CNCs were blended with the suspensions. The nanocomposites were then produced by the direct casting of the homogeneous CNC/TPU suspension in a mold and the subsequent removal of the solvents. Alternatively, the nanocomposites have also been produced via a compression-molding process.[21]

In general, the mechanical properties of CNC/TPU nanocomposites (e.g., E and σ_T) increased 20–80% without sacrificing the strain to failure (ε_f) at low CNC contents (0.25–1.5 wt %). With higher CNC loadings, E continued to increase, but ε_f began to decrease (embrittlement) because of CNC agglomeration.[14,17,19–21] In contrast, Pei *et al.*[16] fabricated CNC/TPU nanocomposites with up to 5 wt % CNC loadings via the two-step polymerization process and reported 450–500% increases in both E and σ_T, while a high ε_f was still maintained. In this case, the CNCs were covalently bonded with specific sites of the hard segment within the TPU, and this resulted in the strengthening of the interfacial bonding between CNCs and TPU. We believe that this resulted in the increased strength and toughness of the composite. Note that when the CNC loading was over the saturation concentration (optimal condition) within the TPU matrix; the excess CNCs began to agglomerate or formed a network structure. This resulted in impedance of the polymer chain movement, and the composite ε_f was expected to decrease (e.g., increase embrittlement). To date, there have not been any studies that have directly blended CNCs within commercialized medically used TPUs and assessed the role of CNC additions on the thermomechanical performance of the resulting nanocomposites.

In TPU fabrication to make products (e.g., extrusion and injection molding), in many cases, high temperatures and long manufacturing time (e.g., blending and homogenization) were applied. These factors degraded the polymer chains and resulted in a decrease in the mechanical properties. If TPUs can achieve a higher decomposition temperature, they will be able to be processed under a wider range of operation temperatures and manufacturing times without a loss of mechanical properties. Thus, the objective of this study was to directly disperse high-solid loadings of CNCs in a commercial TPU [Pellethane 2363-55D (P55D), commonly used in biomedical applications as it has good biocompatibility and oxidative and hydrolytic biostability] to increase the decomposition temperature of the nanocomposites without any sacrifice of the mechanical performance.

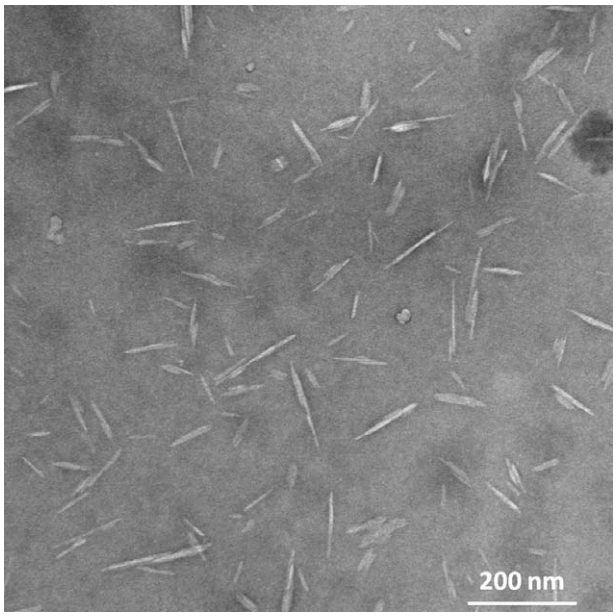

Figure 1. TEM image of freeze-dried CNCs that were redispersed in deionized water and stained with aqueous uranyl acetate.

EXPERIMENTAL

Materials

Freeze-dried CNCs with 0.96 wt % sulfate half-ester (Na^+) on the CNC surface and derived from machine dried prehydrolysis kraft rayon-grade dissolving wood pulp were provided by the Forest Product Laboratory. The detailed manufacturing process can be found elsewhere.[22] The morphology of the CNCs was characterized with transmission electron microscopy (TEM; Philips CM-100, at 100 kV, spot 3, 200-μm condenser aperture, and 50-μm objective aperture). The CNCs were deposited on TEM grids (400-mesh Formvar/carbon filmed grids prepared with blow discharge) with 2% aqueous uranyl acetate stain. Figure 1 shows the rodlike morphology of the CNCs, and their average length was 75 ± 38 nm and average width was 9 ± 3 nm, as determined with ImageJ software for 300 of individual CNC crystals. P55D (Lubrizol), a type of TPU, was used as received. DMF (EMD Chemicals, Saudi Arabia) and dimethylacetamide (DMAc; Sigma Aldrich, Australia) were also used as received.

Nanocomposite Preparation

Nanocomposite films with different CNC solid loadings were fabricated by casting from the solvent. P55D, which was dried at 98°C for 24 h, was dissolved in DMF to prepare a 3 wt % solution. The freeze-dried CNCs were sonified for 3 min to redisperse them in DMAc with a high-energy ultrasonic probe (Branson Sonifier 250) to prepare 40 g of a 2 wt % CNC/DMAc suspension. The output control and duty cycle for sonication were 4 and 80%, respectively. Different quantities of CNC/DMAc suspensions were then added to the P55D/DMF suspensions and stirred for 24 h to obtain a homogeneous mixtures. The mixed suspensions were then cast onto glass Petri dishes and dried at 60°C under an argon atmosphere for an initial 3 h and then dried *in vacuo* for another 12 h to remove residual solvents. The dried films were then annealed at 85°C

for 5 h. A thermal compression cycle was used to minimize the surface roughness; during this cycle, the films were compressed between two copper plates at 160°C under 500 Psi for 30 s. During cooling, the pressure was released at 100°C. After that, these films were annealed again at 85°C for 5 h to remove the thermal stress built within the films. The neat P55D film was prepared with the same process as the nanocomposite films. The CNC-reinforced P55D nanocomposite films with 1, 2, and 5 wt % CNC contents were designated as P55D, P55D/CNC-1, P55D/CNC-2, and P55D/CNC-5, respectively.

Techniques

Mechanical Testing. Tensile testing was carried out with a universal tensile testing machine (MTS Insight, MTS System Corp.), and five replicates were tested for each material condition. Dumbbell samples were punched from the molded sheet stock with a 14-mm gauge length, 2-mm width, and 0.1–0.3-mm thickness. A 1000-N load cell was used for testing, and the crosshead speed was 50 mm/min.

The results are expressed as means plus or minus the standard deviations. Comparisons of the means were performed with the Student *t* test on Microsoft Excel, where two tails (two-tailed distribution) and two-sample equal variance were chosen as function arguments. A value of $p < 0.05$ was taken as significant.

Differential Scanning Calorimetry (DSC). DSC curves of the neat P55D and nanocomposites were measured with a TA Instruments Q100 (TA Instruments) in a helium atmosphere with samples (5–6 mg) sealed in Tzero aluminum pans. After the samples were equilibrated at −100°C, they were heated to 250°C and then cooled down to −100°C at a 10°C/min ramping rate.

Thermogravimetric Analysis (TGA). TGA was carried out on a TA2000 (TA Instruments). The P55D, CNC film, and CNC nanocomposites with 10–15 mg CNCs were loaded into alumina crucibles and tested from 25 to 600°C at a 10°C/min heating rate under a nitrogen atmosphere.

Dynamic Mechanical Analysis (DMA). DMA measurement was performed on a TA Instruments Q800 instrument under tension. The P55D and nanocomposites were prepared in strips with 4–5-mm gauge lengths, 1.8-mm widths, and 0.07–0.1-mm thicknesses. The samples were gripped with clamps and equilibrated at −100°C for 5 min. After that, samples were stretched with a 0.1-N preload force and tested in isostrain/multifrequency mode in the temperature range from −100 to 110°C at a 2°C/min heating rate. The frequency was 2 Hz, and the strain sweep was 0.1% during the test.

RESULTS AND DISCUSSION

CNC/P55D Nanocomposites

The P55D and P55D/CNC nanocomposite films 100–120 μm in thickness were produced by solvent casting processing. The nanocomposite films had a similar transparence compared to the P55D film (Figure 2); this suggested that the freeze-dried CNCs were dispersed in the matrix without having agglomerates in the millimeter and micrometer size scale in the matrix. The

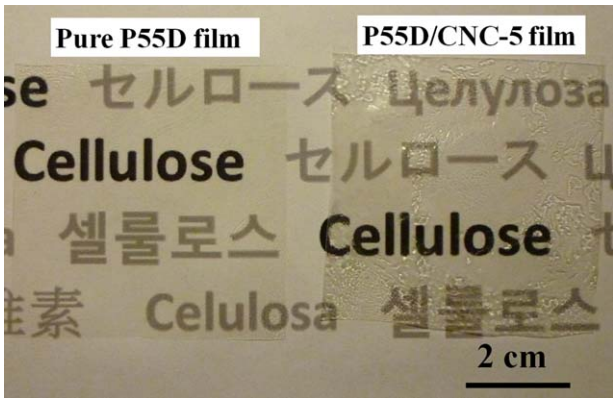

Figure 2. Images of the P55D and P55D/CNC-5 nanocomposite films. [Color figure can be viewed in the online issue, which is available at wileyonlinelibrary.com.]

P55D film had a slightly rough surface; this was due to the fast drying process. However, the nanocomposite films had more surface wrinkles; this increased with higher CNC contents (e.g., P55D/CNC-5 in Figure 2). The rougher surface of the nanocomposite films might have resulted from the hydrophilic CNCs with large surface areas having adsorbed moisture and then having interacted with the P55D during the casting and drying processes.

DSC Analysis

The physical transformation (phase-transition) temperatures of the TPUs, which consisted of different types of soft segments, average lengths, and ratios of hard-to-soft segments, were well studied via DSC.[23–26] The soft/hard segment morphology, the glass-transition temperature (T_g) of both soft and hard segments, and the melting temperature of the hard segment, depending on the degree of crystallinity, were all demonstrated in these studies. Moreover, the P55D was also compared to the TPUs with different soft/hard segment compositions.[25] As a result, the phase transition and degree of crystallization corresponding to different hard domain melting temperatures of the nanocomposites were studied via DSC thermograms.

As shown in Figure 3, the T_g of both the soft and hard domains of P55D that were expected (∼−40 and ∼ 60°C, respectively) were not obvious in the heating curve. There were three melting endotherm regions around 100, 175, and 220°C. These regions with different melting temperatures were attributed to different types of paracrystalline hard segments and were composed of reacted diisocyanates and short chain extender.[23,24] The high-temperature melting (220°C) was assigned to the melting of the longer hard segments with a higher relative crystallinity and order. In contrast, the hard segments with shorter chains only formed partially crystalline regions consisting of a more disordered structure (e.g., random chain folding and agglomerates), and this led to lower melting points. The melting of these lower crystallinity regions was attributed to the first two endotherm regions at lower temperatures (100–200°C).[23–26] After the CNCs were dispersed into the P55D, the high-crystallinity, high-melting-point region completely disappeared, regardless of the CNCs content; this resulted from the CNCs having disturbed

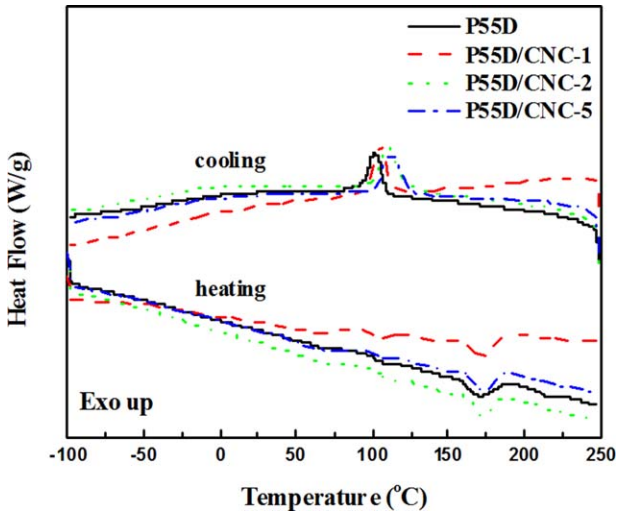

Figure 3. DSC thermograms for the P55D and nanocomposites with 1 wt % CNC (P55D/CNC-1), 2 wt % CNC (P55D/CNC-2), or 5 wt % CNC (P55D/CNC-5). [Color figure can be viewed in the online issue, which is available at wileyonlinelibrary.com.]

the packing of the long polymer chains during the drying process and possibly indicated a specific interaction with the hard blocks. However, all of the nanocomposites still had similar enthalpies of fusion (5.6–6.3 J/g) in the lower crystallinity regions. In the cooling curves, all of the samples showed one crystallization peak, and the enthalpy for crystallization was also similar (12–15 J/g). However, the crystallization temperature shifted to higher temperatures with increasing CNC content in the matrix. The CNCs dispersed in the matrix were considered to be heterogeneous nucleation sites to favor crystallization; this resulted in the crystallization peak of P55D/CNC-5 shifting to higher temperature in the cooling curve. Overall, the CNCs dispersed in the P55D matrix only hindered longer polymer chain packing to form highly crystalline regions, but they also acted as nucleants to assist in the crystallization of the hard segments.

DMA

The dynamic mechanical behavior and damping capacity of the P55D and nanocomposites were studied with DMA. Figure 4 shows the temperature dependence of the storage modulus (E') and loss tangent (tan δ) of the P55D and nanocomposites. As shown in Figure 4(a), E' of the P55D decreased with increasing temperature, and it dropped significantly near the relaxation transition region corresponding to T_g [the onset temperature (T_{on}) where E' decreased]. The E' and T_g (−38 to −41°C) of P55D were minimally affected by low CNC additions (1–2 wt % CNCs). However, P55D/CNC-5 showed slightly increased E' and T_g (∼−34°C) values. As a result, at low CNCs loadings, the viscoelasticity of the nanocomposites was not influenced by the CNCs. However, at higher loadings (5 wt %), the chain movement was hindered. Additionally, in Figure 4(b), the peak temperatures of tan δ of the P55D and nanocomposites (28–30°C), which were associated with the phase transition and damping capacity of the P55D, were also not highly affected by the CNC additions. However, the broadening of the tan δ peak with increasing CNC content demonstrated a lower concentration of

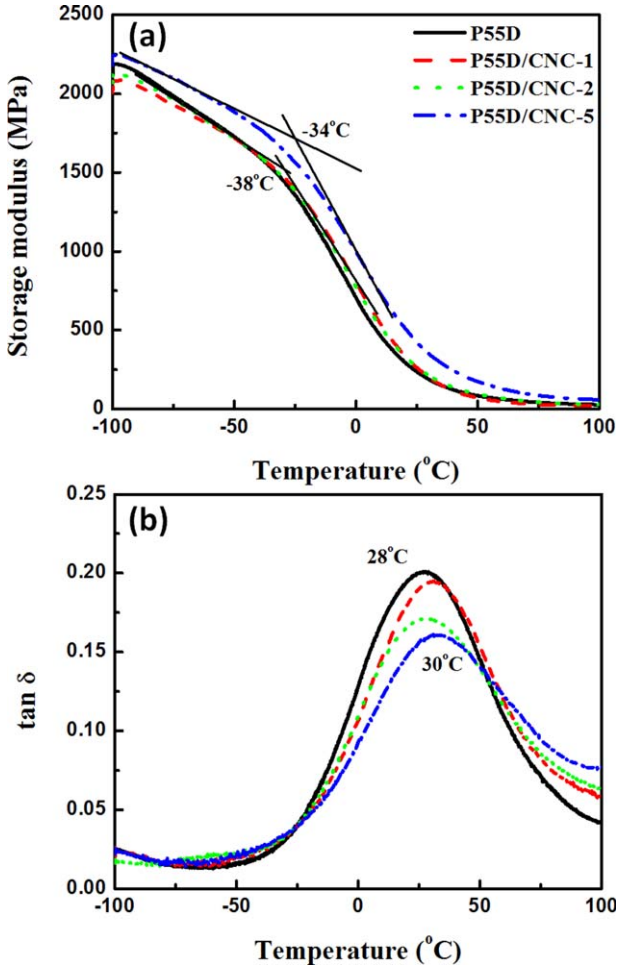

Figure 4. (a) E' and (b) tan δ values of the P55D and nanocomposites with 1 wt % CNC (P55D/CNC-1), 2wt % CNC (P55D/CNC-2), or 5 wt % CNC (P55D/CNC-5) as a function of the temperature. [Color figure can be viewed in the online issue, which is available at wileyonlinelibrary.com.]

amorphous soft segments participating in phase transformation. The two-dimensional microdomain (soft and hard domains) morphology of P55D was generated as two continuous phases in a previous study.[25] The size of hard doamins were on the order of 5–10 nm; this suggested that the much larger CNCs could be tethered between hard domains (spaned across soft domains and interfacial region), and this reduced the mobility of the soft domains. Moreover, at higher CNC concentrations (e.g., 5 wt %), the chain mobility of both the hard and soft segments could be further reduced as there was a higher density of CNCs in the matrix as compared to that at low CNC concentrations. This resulted in a slight increase in E' and T_g of the nanocomposite.

Decomposition Behavior

The decomposition behavior of P55D and nanocomposites as a function of the temperature was analyzed by TGA. In the thermogravimetry (TG) curves [Figure 5(a)], the CNC film had an initial weight loss around 100°C; this was attributed to the absorbed water within the film, and it followed a main decomposition around 260°C, which resulted from the breaking of cellulose chains. In contrast to the CNC film decomposition, the

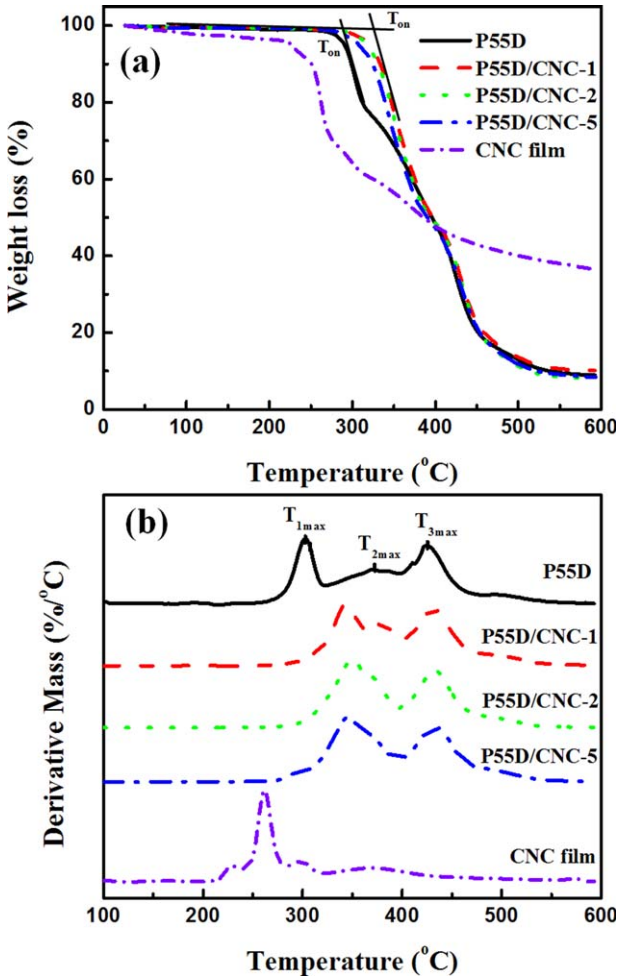

Figure 5. (a) TG and (b) derivative curves of the P55D; nanocomposites with 1 wt % CNC (P55D/CNC-1), 2 wt % CNC (P55D/CNC-2), or 5 wt % CNC (P55D/CNC-5); and CNC film. [Color figure can be viewed in the online issue, which is available at wileyonlinelibrary.com.]

P55D and nanocomposites displayed two distinct regions of weight loss. When we looked at the extrapolated T_{on} that denoted the temperature where the weight loss began, the nanocomposites had a higher T_{on} than P55D. The two distinct regions were more obviously reflected in the two main decomposition stages in the derivative curves [Figure 5(b)]. The first stage (~300°C) was attributed to decomposition of hard domains (urethane bonds) of the polyurethane where the maximum peak temperature was T_{1max}. The second stage, which consisted of two peaks (~370 and 430°C), was related to the decomposition of the soft domains,[27,28] and the maximum temperatures of the peaks were T_{2max} and T_{3max}, respectively. Table I summarizes the T_{on} and maximum peak temperatures (T_{1max}, T_{2max}, and T_{3max}) of the P55D and nanocomposites. T_{on} and T_{1max} increased with CNC addition; however, there was no further increases in T_{on} and T_{1max} at contents higher than 1 wt % CNC in the matrix, although this was the lowest CNC content studied. Unlike T_{on} and T_{1max}, T_{2max} and T_{3max} were independent of the CNC content. The CNCs in the nanocomposites only influenced the decomposition process of the soft domain; this resulted in a fluctuating T_{2max} temperature (large standard deviation), but the T_{3max} was similar. T_{2max} and T_{3max} of the P55D and nanocomposites were statistically the same. The unchanged T_{2max} and T_{3max} suggested that the CNCs had little interaction with the soft domains of P55D. The delayed decomposition temperature (high T_{on} and T_{1max}) of the nanocomposites may have been due to the formation of hydrogen bonds between the hydroxyl groups on the CNC surface and urethane groups (hard domains) of P55D stabilizing the urethanes. As the urethane bonds were the first to break on thermolysis, their extra stability in the presence of the CNCs led to a higher T_{on}. The high surface area of the CNCs may have had more bondable hydroxyl groups compared to urethane groups; as a result, at very low CNC contents, most of the urethane groups were already bonded. At higher CNC contents, unbound CNCs may have begun to agglomerate, and this resulted in a less efficient utilization of the CNCs (no further increase in the decomposition temperature).

Mechanical Properties

Representative stress–strain curves and tensile properties (E, σ_T, and ε_f) of the P55D and nanocomposites are shown in Figure 6 and Table I, respectively. E was calculated from the initial slope of the stress–strain curves at about a 0–5% strain. All of the samples showed the same elastomeric behavior, where the stress linearly increased at a small deformation and then increased with large plastic deformation (high elongation; Figure 6). In Table I, when we compared the tensile properties of P55D ($E = 45 \pm 6$ MPa, $\sigma_T = 54 \pm 12$ MPa, and $\varepsilon_f = 384 \pm 91\%$) to that of nanocomposites, there were increases in the E values of P55D/CNC-1 ($E = 55 \pm 3$ MPa), P55D/CNC-2 ($E = 68 \pm 14$ MPa), and P55D/CNC-5 ($E = 76 \pm 16$ MPa) of 22, 56, and 76%, respectively, whereas there were no significant changes ($p > 0.05$) in σ_T (53–69 MPa) and ε_f (360–416%). The work of fracture of P55D and nanocomposite was also statistically the same ($p > 0.05$, 100–155 MJ/m^3).

The stiffness and ductility in nanocomposites are often mutually exclusive properties, where an increasing modulus typically also embrittles a material. However, as shown in Table I, the E of the nanocomposites increased with increasing CNC content without compensating the ductility of P55D. On the basis of the DSC, DMA, and TGA results, we considered that the CNCs formed hydrogen bonds with the urethane groups and tethers/bridges among the hard-domain phases. The tethering reduced the soft-segment mobility and increased the stress value at low strains (0–50%) at high CNC loadings; this explained the higher stress value of P55D/CNC-2 and P55D/CNC-5 at low strains shown in Figure 6. However, even though polymer chains were restrained due to tethering, CNCs were still able to rotate enabling plastic flow under tensile deformation. Therefore, there was no loss in the elongation to break of the nanocomposites.[29] Additionally, the hydrogen bonding around the hard segment increased the stiffness of the nanocomposites. This promising result demonstrated that the CNCs could be used as a reinforcement to increase E while maintaining the ductility of the P55D matrix. Alternatively, at low CNC loadings, the stiffness was not obviously affected (as the CNCs were primarily loaded in the hard-segment domains); this may be important for soft TPU applications.

Table I. Thermal Decomposition Temperatures, Mechanical Properties, and Work of Fracture of P55D and CNC Nanocomposites

	Thermal decomposition temperature			
	T_{on} (°C)	T_{1max} (°C)	T_{2max} (°C)	T_{3max} (°C)
P55D	286 ± 3	300 ± 2	372 ± 6	428 ± 4
P55D/CNC-1	327 ± 4	347 ± 3	369 ± 13	432 ± 2
P55D/CNC-2	324 ± 2	349 ± 1	367 ± 1	433 ± 1
P55D/CNC-5	318 ± 3	344 ± 2	362 ± 5	431 ± 1

	Mechanical properties			
	E (MPa)	σ_T (MPa)	ε_f (%)	Work of fracture (MJ/m^3)
P55D	45 ± 6	54 ± 12	384 ± 91	112 ± 48
P55D/CNC-1	55 ± 3	53 ± 7	360 ± 44	101 ± 25
P55D/CNC-2	68 ± 14	69 ± 11	416 ± 57	155 ± 42
P55D/CNC-5	76 ± 16	65 ± 9	390 ± 34	134 ± 32

As a comparison of the experimental results and estimated nanocomposite elastic properties, the micromechanics did not work so well to estimate the nanocomposite elastic properties. Clearly, some of the assumptions needed were not met, such as perfect interfaces and load transfer between the different phases, perfect one-dimensional orientation of the CNCs within the composite (most likely, we had two-dimensional random CNC orientation within the film), and the estimate of input values for the elastic properties of each phase may have been in error. Note that the CNC E was anisotropic and was shown to vary from 15 to 220 GPa, depending on the direction of measurement.[30] Additionally, the TPU nanocomposites were very complex because soft rubbery domains preferentially dominated the deformation; this allowed the nanoscale discrete hard domains to rotate upon the application of strain, and thus, their component in the stiffness of the composite changed with the degree of orientation.

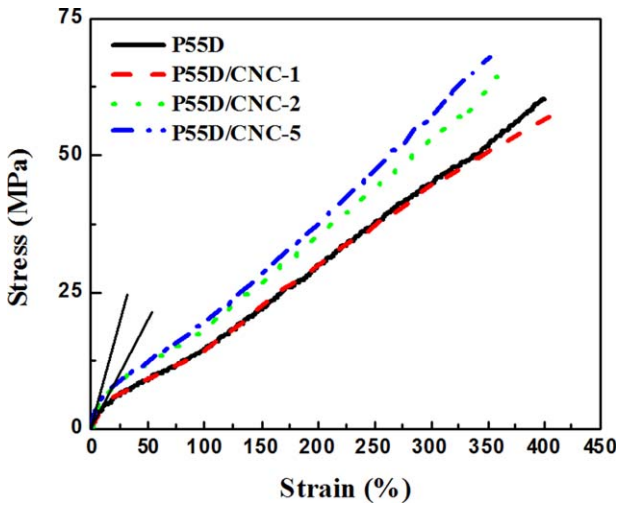

Figure 6. Representative stress–strain curves of the P55D and CNC nanocomposites. The dashed lines represent the E values of the P55D and nanocomposites. [Color figure can be viewed in the online issue, which is available at wileyonlinelibrary.com.]

The mechanical performance of the polyurethane (PU) nanocomposites varied with the material system, nanofillers, dispersion of nanofillers, and fabrication process. Table II compares the enhanced mechanical properties (e.g., E, σ_T, and ε_f) of the biocompatible nanocomposites fabricated from commercialized PUs or PUs with the potential to be developed as biomedical devices with nontoxic nanofillers (e.g., layered silicates or organically modified silicates). The percentage changes in the mechanical properties are listed in the table to highlight the influence of the nanofillers on the mechanical properties of the nanocomposites at the optimized addition.

Poly(urethane urea) (PUU) nanocomposites may allow higher additions of organically modified silicates (e.g., 20 wt %) dispersed in the matrix with a 160–240% increase of E, and σ_T and ε_f were maintained with the same properties or had a 36–54% increase.[31,32] In the poly(ether urethane) (PEU) nanocomposites, the optimized nanofiller content varied from 4 to 15 wt %.[33–35] At a high addition (e.g., 15 wt %) of montmorillonite (MMT), E showed an obvious 170% increase, but the strength decreased by 45%. Although the nanocomposite obtained a greater improvement in E with a better dispersion of organically modified MMT, the strength decreased further.[33] The fabrication process also influenced the mechanical performances of the nanocomposite. Cloisite 30B had a greater interaction with the PU matrix and better dispersion when the nanoparticles with polyol were added before the polymerization process. This resulted in a high E and toughness of the nanocomposite (e.g., 430% increase in E). Stiffer nanocomposites were fabricated by the addition of nanoclay after the polymerization process and showed a 1700% increase in E but a 67% reduction in ε_f.[34] In other types of polyurethane nanocomposites, only small amounts of silicates (2 wt %) were able to be dispersed in the matrix to obtain a high E (a 45% increase) without a loss of ε_f.[36,37]

Table II. Improvements in the Mechanical Properties of Nontoxic Polyurethane Nanocomposites with Optimized Nanofiller Contents

Nanofiller	Polyurethane	Optimized nanofiller addition (wt %)	E (%)	σ_T (%)	ε_f (%)
PUU					
Cloisite 15A[31]	BioSpan[31]	20	170[a]	N/A	N/A
Cloisite 15A[32]	Synthesized PUU	20	240[a]	36	54
Nanomer I.30TC[31]	BioSpan MS/0.4	20	160[a]	N/A	N/A
PEU					
CNC	P55D	5	70	N/A	N/A
MMT[33]	Company supply	15	170	−45	N/A
Modified MMT[33]	Company supply	15	245	−50	N/A
Cloisite 30B[34]	Synthesized PEU	4	430[c]	—	33[c]
Cloisite 30B[34]	Synthesized PEU	4	1700[d]	—	−67[d]
Cloisite 30B[35]	Tecoflex EG 80A	5	23[b]	150	25
Other types of polyurethane					
Cloisite 30B[36]	Synthesized PU	2	120	N/A	−70
Modified ME100[37]	ElastEon E5-325	2	45	N/A	20
Modified lucentite[37]	ElastEon E5-325	2	45	20	15

N/A, no significant change.
[a] Modulus at 50% elongation.
[b] Modulus at 300% elongation.
[c] The nanofiller was initially mixed with polyol, and then, the polymerization process followed.
[d] The nanofiller was added to the matrix after polymerization.

In contrast to the these nontoxic nanocomposites, the P55D/CNC nanocomposites (Table II) showed an increase in E with increasing CNC, with a marginal increase at low loadings rising to a 70% increase in E with 5 wt % nanofiller content, all without losses in the strength or ε_f. Thus, the CNCs could tune the modulus, maintain the elongation, and at low loadings, increase the thermal degradation temperature and so may ultimately be most useful as a thermal stability additive for TPUs. Moreover, CNC-reinforced nanocomposites have potential in a greater improvement of the mechanical properties with an increased addition of CNCs in the matrix.

CONCLUSIONS

Freeze-dried CNCs were redispersed in P55D to fabricate nanocomposites via solvent casting, where the resulting nanocomposite films were transparent with a rough surface. With increasing CNC content, the E', phase-transition temperature (e.g., T_g and tan δ peak temperature), and endotherm and exotherm behaviors of the nanocomposites showed no obvious changes, although the tan δ peak was broadened with the addition of 2–5 wt % CNCs. Importantly, the increased onset of thermal degradation of nanocomposites was shown upon the addition of as little as 1 wt % CNCs (our lowest level of addition). The increased decomposition temperature (T_{on} and T_{1max}) of the nanocomposites, we believe, was due to the formation of hydrogen bonds between the CNCs and urethane groups (hard domains) of P55D; this, thereby, stabilized them. Low CNC loadings showed no obvious effect on the strength or elongation of the P55D. As the loadings were increased, about a 70% increase in the tensile modulus compared to that of P55D was observed without a compromise of the elongation (i.e., no embrittlement). We considered that CNC-tethered hard-domain phases resulted in a hindered mobility of the soft segment (an increased stress value) at low strains at high loadings; however, CNCs were still free to rotate and flow in the matrix under tensile deformation. This preserved the ε_f values of the nanocomposites. As a result, the higher onset degradation temperature of the nanocomposite provided a wider processing temperature for manufacturing products to be used in biomedical devices without a loss of mechanical properties in the nanocomposites.

ACKNOWLEDGMENTS

The authors thank the Seed Grant for Purdue/University of Queensland Early Career Researcher Exchange Travel Grant for funding this project. They are also grateful to the Forest Products Laboratory (U.S. Forest Service) for providing the freeze-dried CNCs. The authors also appreciate Darren Martin's research group at the Australian Institute for Bioengineering and Nanotechnology (University of Queensland, Australia) for its support with research materials and equipment.

REFERENCES

1. Mallikarjuna, S. R.; Sivaram, S. Thermoset Nanocomposites; Wiley-VCH: Weinheim, **2013**; Chapter 3, p 39.

2. Martin, D. J.; Osman, A. F.; Andriani, Y.; Edwards, G. A. Advances in Polymer Nanocomposites: Types and Applications; Elsevier Science: Amsterdam, **2012**; Chapter 11, p 321.

3. Njuguna, J.; Pielichowski, K.; Desai, S. *Polym. Adv. Technol.* **2008**, *19*, 947.
4. Moon, R. J.; Martini, A.; Nairn, J.; Simonsen, J.; Youngblood, J. *Chem. Soc. Rev.* **2011**, *40*, 3941.
5. Lin, N.; Dufresne, A. *Eur. Polym. J.* **2014**, *59*, 302.
6. Diaz, J. A.; Wu, X. W.; Martini, A.; Youngblood, J. P.; Moon, R. *J. Biomacromolecules* **2013**, *14*, 2900.
7. Miao, C. W.; Hamad, W. Y. *Cellulose* **2013**, *20*, 2221.
8. Eichhorn, S.; Dufresne, A.; Aranguren, M.; Marcovich, N.; Capadona, J.; Rowan, S.; Weder, C.; Thielemans, W.; Roman, M.; Renneckar, S.; Gindl, W.; Veigel, S.; Keckes, J.; Yano, H.; Abe, K.; Nogi, M.; Nakagaito, A.; Mangalam, A.; Simonsen, J.; Benight, A.; Bismarck, A.; Berglund, L.; Peijs, T. *J. Mater. Sci.* **2010**, *45*, 1.
9. Pan, H. F.; Song, L.; Ma, L. Y.; Hu, Y. *Ind. Eng. Chem. Res.* **2012**, *51*, 16326.
10. Liu, H. Y.; Liu, D. G.; Yao, F.; Wu, Q. L. *Bioresour. Technol.* **2010**, *101*, 5685.
11. Yu, H. Y.; Qin, Z. Y.; Liu, Y. N.; Chen, L.; Liu, N.; Zhou, Z. *Carbohydr. Polym.* **2012**, *89*, 971.
12. Visakh, P. M.; Thomas, S.; Oksman, K.; Mathew, A. P. *Compos. A* **2012**, *43*, 735.
13. Bahar, E.; Ucar, N.; Onen, A.; Wang, Y. J.; Oksuz, M.; Ayaz, O.; Ucar, M.; Demir, A. *J. Appl. Polym. Sci.* **2012**, *125*, 2882.
14. Auad, M. L.; Mosiewicki, M. A.; Richardson, T.; Aranguren, M. I.; Marcovich, N. E. *J. Appl. Polym. Sci.* **2010**, *115*, 1215.
15. Rueda, L.; Saralegi, A.; Fernandez-d'Arlas, B.; Zhou, Q.; Alonso-Varona, A.; Berglund, L. A.; Mondragon, I.; Corcuera, M. A.; Eceiza, A. *Cellulose* **2013**, *20*, 1819.
16. Pei, A. H.; Malho, J. M.; Ruokolainen, J.; Zhou, Q.; Berglund, L. A. *Macromolecules* **2011**, *44*, 4422.
17. Rueda, L.; Saralegui, A.; Fernandez d'Arlas, B.; Zhou, Q.; Berglund, L. A.; Corcuera, M. A.; Mondragon, I.; Eceiza, A. *Carbohydr. Polym.* **2013**, *92*, 751.
18. Saralegi, A.; Rueda, L.; Martin, L.; Arbelaiz, A.; Eceiza, A.; Corcuera, M. A. *Compos. Sci. Technol.* **2013**, *88*, 39.
19. Rueda, L.; Fernandez d'Arlas, B.; Zhou, Q.; Berglund, L. A.; Corcuera, M. A.; Mondragon, I.; Eceiza, A. *Compos. Sci. Technol.* **2011**, *71*, 1953.
20. Auad, M. L.; Contos, V. S.; Nutt, S.; Aranguren, M. I.; Marcovich, N. E. *Polym. Int.* **2008**, *57*, 651.
21. Floros, M.; Hojabri, L.; Abraham, E.; Jose, J.; Thomas, S.; Pothan, L.; Leao, A. L.; Narine, S. *Polym. Degrad. Stab.* **2012**, *97*, 1970.
22. Reiner, R. S.; Rudie, A. W. Production and Applications of Cellulose Nanomaterials; TAPPI Press: Peachtree Corners, GA, **2013**; Chapter 1.1, p 21.
23. Martin, D. J.; Meijs, G. F.; Gunatillake, P. A.; McCarthy, S. J.; Renwick, G. M. *J. Appl. Polym. Sci.* **1997**, *64*, 803.
24. Martin, D. J.; Meijs, G. F.; Renwick, G. M.; McCarthy, S. J.; Gunatillake, P. A. *J. Appl. Polym. Sci.* **1996**, *62*, 1377.
25. Martin, D. J.; Meijs, G. F.; Gunatillake, P. A.; Yozghatlian, S. P.; Renwick, G. M. *J. Appl. Polym. Sci.* **1999**, *71*, 937.
26. Seymour, R. W.; Cooper, S. L. *Macromolecules* **1973**, *6*, 48.
27. Trovati, G.; Ap Sanches, E.; Neto, S. C.; Mascarenhas, Y. P.; Chierice, G. O. *J. Appl. Polym. Sci.* **2010**, *115*, 263.
28. Petrovic, Z. S.; Zavargo, Z.; Flynn, J. H.; Macknight, W. J. *J. Appl. Polym. Sci.* **1994**, *51*, 1087.
29. Osman, A. F.; Andriani, Y.; Edwards, G. A.; Schiller, T. L.; Jack, K. S.; Morrow, I. C.; Halley, P. J.; Martin, D. J. R. *Soc. Chem. Adv.* **2012**, *2*, 9151.
30. Dri, F.; Hector, L. G.; Moon, R. J.; Zavattieri, P. *Cellulose* **2013**, *20*, 2703.
31. Xu, R. J.; Manias, E.; Snyder, A. J.; Runt, J. *J. Biomed. Mater. Res. A* **2003**, *64*, 114.
32. Xu, R. J.; Manias, E.; Snyder, A. J.; Runt, J. *Macromolecules* **2001**, *34*, 337.
33. Styan, K. E.; Martin, D. J.; Poole-Warren, L. A. *J. Biomed. Mater. Res. A* **2008**, *86*, 571.
34. Mishra, A.; Das Purkayastha, B. P.; Roy, J. K.; Aswal, V. K.; Maiti, P. *Macromolecules* **2010**, *43*, 9928.
35. Barick, A. K.; Tripathy, D. K. *J. Appl. Polym. Sci.* **2010**, *117*, 639.
36. Rueda, L.; Garcia, I.; Palomares, T.; Alonso-Varona, A.; Mondragon, I.; Corcuera, M.; Eceiza, A. *J. Biomed. Mater. Res. A* **2011**, *97*, 480.
37. Osman, A. F.; Edwards, G. A.; Schiller, T. L.; Andriani, Y.; Jack, K. S.; Morrow, I. C.; Halley, P. J.; Martin, D. *J. Macromolecules* **2012**, *45*, 198.